Investigations of the ambiguity effect in the estimation of Doppler frequency and directions in channel sounding using switched Tx and Rx arrays

Pedersen, Troels; Pedersen, Claus; Yin, Xuefeng; Fleury, Bernard Henri; Pedersen, R.R.; Bozinovska, B.; Hviid, A.; Jourdan, P.; Stucki, A.

Publication date:
2004

Document Version
Publisher's PDF, also known as Version of record

EUROPEAN COOPERATION
IN THE FIELD OF SCIENTIFIC
AND TECHNICAL RESEARCH

EURO-COST

COST 273 TD(04)021
Athens, Greece
2004/Jan/26-28

SOURCE: Digital Communications Division,
Department of Communication Technology,
Aalborg University,
Denmark

Investigations of the Ambiguity Effect in the Estimation of Doppler Frequency and Directions in Channel Sounding Using Switched Tx and Rx Arrays

Troels Pedersen, Claus Pedersen, Rene R. Pedersen, Biljana Bozinovska,
Asger Hviid, Xuefeng Yin, Bernard H. Fleury,
Digital Communications Division,
Department of Communication Technology, Aalborg University,
DK-9220 Aalborg, Denmark
Phone ++ 45 96 35 86 72
Fax: ++ 45 98 15 15 83
Email: tped00@kom.auc.dk, cped00@kom.auc.dk, xuefeng@kom.auc.dk

Patrik Jourdan, Andreas Stucki
Elektrobit AG, Rosswiesstrasse 29, CH-8608 Bubikon,
Switzerland

Investigations of the Ambiguity Effect in the Estimation of Doppler Frequency and Directions in Channel Sounding Using Switched Tx and Rx Arrays

Troels Pedersen*, Claus Pedersen*, Xuefeng Yin*, Bernard H. Fleury*,
Rene R. Pedersen*, Biljana Bozinovska*, Asger Hviid*, Patrik Jourdan**, Andreas Stucki**
*Digital Communications Division, Department of Communication Technology,
Aalborg University, DK-9220 Aalborg, Denmark
**Elektrobit AG, Rosswiesstrasse 29, CH-8608 Bubikon, Switzerland

***Abstract*— The improved-search-and-initialization space-alternating generalized expectation-maximization (ISI-SAGE) algorithm is proposed in [1] and [2] for joint estimation of the relative delay, the direction (i.e. azimuth and co-elevation) of departure, the direction of arrival, the Doppler frequency (DF) as well as the complex weight of the propagation paths from the transmitter (Tx) site to the receiver (Rx) site in mobile radio environments. A recent study [3] shows that the ISI-SAGE algorithm combined with a switched multiple-element Tx and Rx antenna sounding technique makes it possible to estimate the DF with an absolute value up to half the rate with which the pairs of Tx and Rx elements are switched (switching rate), rather than half the rate with which any fixed pair is switched (cycle rate) as commonly believed. This paper shows that so-called modulo-type switching modes (SMs) used with uniform linear and planar arrays lead to an ambiguity in the estimation of the DF and the directions, when the DF estimation range is extended from minus to plus half the switching rate. The SM of a switched array is the order with which the array elements are switched. Moreover, theoretical and experimental investigations show that the ambiguity problem can be avoided by using some specific SMs.**

I. Introduction

Deploying multiple-element antennas at the transmitter (Tx) and the receiver (Rx) combined with space-time coding can substantially increase the capacity of mobile radio communication systems [4], [5] and [6]. A system or technique using multiple-element Tx and Rx antennas is called a multiple-input multiple-output (MIMO) system or technique. The design and optimization of MIMO communication systems require realistic models of the propagation channel, that incorporate dispersion in direction or equivalently space selectivity jointly at both Tx and Rx sites. High-resolution channel estimation has become an essential tool to extract the critical model parameters from measurement data. The improved-search-and-initialization space-alternating generalized expectation-maximization (ISI-SAGE) algorithm has recently been proposed for joint estimation of the complex weight, relative delay, Doppler frequency (DF), direction, i.e. azimuth and co-elevation angles, of departure (DoD), and direction of arrival (DoA) of propagation paths between the Tx site and the Rx site [2], [7]. Experimental investigations [1] demonstrate the high potential of the algorithm for detailed propagation studies.

MIMO channel sounders commonly operate in a time-division multiplex (TDM) mode in order to save hardware equipment. The sounding signal is fed successively at the inputs of the array elements at the Tx, and while each of these elements transmits, the outputs of the antenna elements at the Rx are sensed successively. A measurement cycle interval is the period separating two consecutive intervals during which a fixed pair of elements at the Tx and Rx is switched. The interval between two consecutive sensing periods is called the switching interval. Notice that the ratio of the cycle interval by the switching interval is at least equal to the product of the numbers of array elements at the Tx and Rx. The cycle rate and the switching rate are the inverses of the cycle interval and the switching interval respectively. It was traditionally believed, that the maximum absolute DF that can be estimated using the TDM-MIMO sounding technique equals half the cycle rate rather than the switching rate. Therefore, by keeping the switching rate unchanged, large numbers of elements in the arrays result in low cycle rates and consequently lead to small DF estimation ranges. However, recent study [3] has shown that the maximum absolute DF that can be estimated using the TDM-MIMO sounding technique actually equals half the switching rate. This implies, that (1) the maximal absolute DF that can be estimated with the TDM-MIMO sounding techniques is larger, actually similar to that achievable with a parallel MIMO sounding technique, and (2) the maximal absolute DF does not depend on the number of elements in the MIMO system. In [3], the above conclusion was drawn based on the assumption that all the wave parameters but the DF and complex amplitude are known. We will show that the above extension of the DF estimation range can result in an ambiguity problem when the directions (DoD and DoA) of the waves are estimated as well if the switching modes (SMs) of the arrays belong to a so-called “modulo-type” class in the case that uniform linear or planar arrays are used. The SM of an array describes the order in which the elements of this array are switched. It turns out that the conventionally used sequential SM in MIMO channel sounder employing uniform linear or planar arrays belongs to this class.

In the ISI-SAGE algorithm, the parameters of each wave are estimated based on a parametric model describing the phase

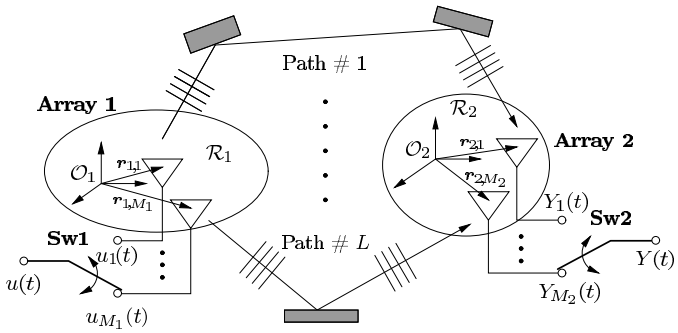

Fig. 1. Signal model for the TDM-MIMO sounding technique.

changes of the signals contributed by the wave among the antenna elements due to its DF, DoA and DoD. The parameter estimates form the solution that maximizes a given objective function. The objective function always exhibits a unique maximum when the DF is confined in the range from minus to plus half the cycle rate. It may exhibit multiple maxima when the DF range is enlarged from minus to plus half the switching rate depending on the selected SMs. The latter effect leads to an ambiguity in the joint estimation of the DoD, DoA, and DF. This paper describes the ambiguity problem, investigates it analytically in a case study (TDM Single-Input Multiple-Output (SIMO)), and shows how the ambiguity can be avoided by appropriately selecting the SMs.

The paper is organized as follows. The MIMO radio channel model is introduced in Section II. Section III presents the model for TDM-MIMO channel sounding. In Section IV the objective function used in the maximization-step of the ISI-SAGE algorithm is derived analytically for the TDM MIMO channel sounding to illustrate and get insight into the ambiguity problem. A case study considering a TDM-SIMO system is also analyzed to demonstrate the ambiguity problem, and a solution to avoid the problem is proposed. In Section V experimental investigations compare the performance of the DF and direction estimators when applying conventional i.e. sequential SMs and optimized SMs to uniform planar array. Finally, concluding remarks are addressed in Section VI.

II. Signal Model for MIMO Systems

Let us consider the propagation environment depicted in Fig. 1. A certain number, L, of waves propagate along different paths for the M_1 Tx antennas forming Array 1 to the M_2 Rx antennas forming Array 2. Along its path a wave interacts with a certain number of scatterers. Following [8], we assume that the far-field condition holds, and that the elements of the Tx and Rx arrays are confined in regions $\mathcal{R}_1$ and $\mathcal{R}_2$ respectively, in which the plane wave approximation is accurate. A coordinate system is specified at an arbitrary origin $\mathcal{O}_k$ in $\mathcal{R}_k$ ($k = 1, 2$). The individual locations of the elements of Array k are then determined by the vectors $\boldsymbol{r}_{k,m} \in \mathbb{R}^3, m = 1, \ldots, M_k$. Here, $\mathbb{R}$ denotes the real line.

Let $\boldsymbol{u}(t) \doteq [u_1(t), \ldots, u_{M_1}(t)]^{\mathrm{T}}$ denote the (complex baseband representation of the) signal vector at the input of Array 1. Here, $[\cdot]^{\mathrm{T}}$ is the transpose operator. The contribution of the ℓth wave to the outputs of Array 2 can be written in vector notation as

$$\boldsymbol{s}(t; \boldsymbol{\theta}_\ell) = \alpha_\ell \exp\{j2\pi\nu_\ell t\} \boldsymbol{c}_2(\boldsymbol{\Omega}_{2,\ell}) \boldsymbol{c}_1(\boldsymbol{\Omega}_{1,\ell})^{\mathrm{T}} \boldsymbol{u}(t - \tau_\ell). \quad (1)$$

In this expression, $\boldsymbol{\theta}_\ell \doteq [\boldsymbol{\Omega}_{1,\ell}, \boldsymbol{\Omega}_{2,\ell}, \tau_\ell, \nu_\ell, \alpha_\ell]$ is a vector of which the entries are the parameters characterizing the ℓth path: $\boldsymbol{\Omega}_{1,\ell}, \boldsymbol{\Omega}_{2,\ell}, \tau_\ell, \nu_\ell$, and α_ℓ denote, respectively its DoD, DoA, propagation delay, DF, and complex weight (or attenuation). We describe a direction as a unit vector $\boldsymbol{\Omega}$ with initial point anchored at the reference location, or equivalently as the terminal point of this vector, i.e. a point located on a unit sphere centered at the reference point. Then, $\boldsymbol{\Omega}$ is uniquely determined by its spherical coordinates $(\phi, \theta) \in [-\pi, \pi) \times [0, \pi]$ according to $\boldsymbol{\Omega} = [\cos(\phi)\sin(\theta), \sin(\phi)\sin(\theta), \cos(\theta)]^{\mathrm{T}}$. The angles ϕ and θ are referred to as, respectively, the azimuth and the co-elevation of $\boldsymbol{\Omega}$. The M_k-dimensional complex vector $\boldsymbol{c}_k(\boldsymbol{\Omega})$ represents the response of Array k ($k = 1, 2$) to a wave impinging from direction $\boldsymbol{\Omega}$ with respect to the reference $\mathcal{O}_k$. Provided coupling effects between the array elements are negligible, $\boldsymbol{c}_k(\boldsymbol{\Omega})$ takes the form $\boldsymbol{c}_k(\boldsymbol{\Omega}) \doteq [f_{k,m}(\boldsymbol{\Omega}) \exp\{j\frac{2\pi}{\lambda_0}(\boldsymbol{\Omega} \cdot \boldsymbol{r}_{k,m})\}; m = 1, \ldots, M_k]^{\mathrm{T}}$. The function $f_{k,m}(\boldsymbol{\Omega})$ is the complex electric field patterns of the mth element in Array k, λ_0 denotes the carrier wavelength and $(\cdot)$ stands for the scalar product.

The signal vector $\boldsymbol{Y}(t) \doteq [Y_1(t), \ldots, Y_{M_2}(t)]^{\mathrm{T}}$ representing the outputs of Array 2 is given by

$$\boldsymbol{Y}(t) = \sum_{\ell=1}^{L} \boldsymbol{s}(t; \boldsymbol{\theta}_\ell) + \sqrt{\tfrac{N_0}{2}} \boldsymbol{W}(t), \quad (2)$$

where $\boldsymbol{W}(t) \doteq [W_1(t), \ldots, W_{M_2}(t)]^{\mathrm{T}}$ is standard M_2-dimensional complex temporally and spatially white Gaussian noise, and N_0 is a positive constant.

III. TDM Channel Sounding Technique

Sounding of the propagation channel is performed in a TDM mode according to the time structure depicted in Fig. 2. The sounding signal is fed via Switch 1 (Sw1 in Fig. 1) to each element of Array 1 during a sounding period T_t. The outputs of the elements of Array 2 are switched successively by Switch 2 (Sw2) with a (switching) interval T_r. Each element is sensed during T_s, where $T_r \geq T_s$. From the figure it is obvious that the relation between T_t and T_r is $T_t = M_2 T_r$. A measurement cycle during which each pair of Tx elements and Rx elements are switched once lasts $M_1 T_t$ seconds. The duration between two consecutive measurement cycles is called the measurement cycle interval and is denoted by T_{cy}. The cycle repetition rate is the ratio $R \doteq \frac{T_{cy}}{M_1 T_t} \geq 1$. Notice that the switching rate T_r^{-1} is related to the measurement cycle rate T_{cy}^{-1} according to $T_r^{-1} = M_1 M_2 R T_{cy}^{-1}$. The guard interval T_g in Fig. 2 is irrelevant in the subsequent investigations. The motivation for introducing it is presented in [7].

To characterize a SM, we need first to define a (spatial) indexing of the array which is then kept fixed. The natural indexing of the elements of a uniform linear array is according to their ordering along the array axis, starting at one end. Similarly the natural indexing of a uniform planar array is according to first the order in the row and second the order inside the row of the array. The SM of Array k can be described for each cycle by a permutation of M_k elements

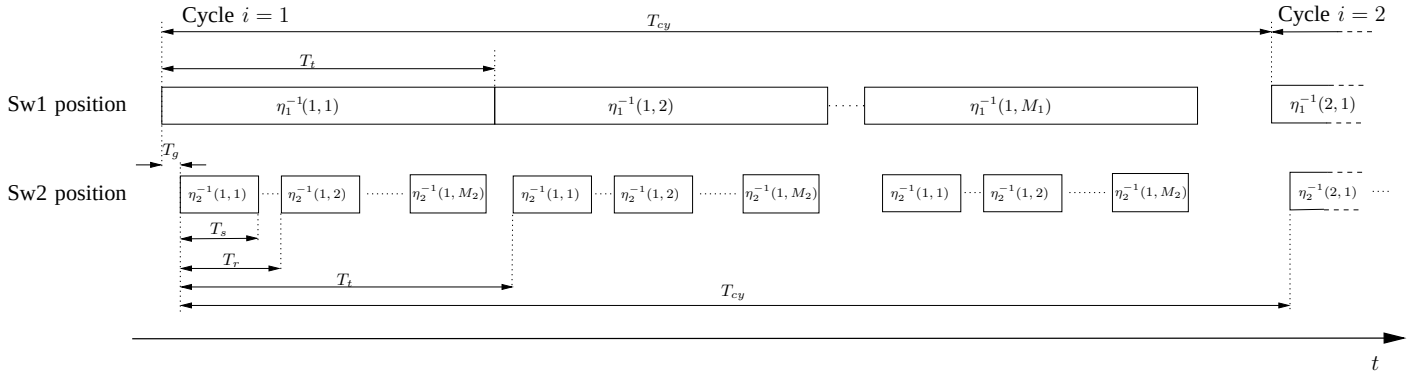

Fig. 2. The considered TDM measurement mode with cycle-dependent space-time mapping scheme.

denoted by $\eta_k(i,m)$ with $m=1,\ldots,M_k$ being the array element index. Clearly, $\eta_k(i,m)$ is the time index of the interval during which the mth element of Array k is switched during the ith cycle. With the above definition, the beginning of the sensing interval for the m_2th element at the Rx while the m_1th element at the Tx is transmitting during the ith cycle is $t_{i,m_1,m_2} \doteq \big(i-\frac{I+1}{2}\big)\,T_{cy}+\big(\eta_1(i,m_1)-\frac{M_1+1}{2}\big)\,T_t+\big(\eta_2(i,m_2)-\frac{M_2+1}{2}\big)\,T_r$. Notice that the permutation $\eta_k(i,m)$ maps the antenna (spatial) index onto a time index. The time-space mapping functions for Array k during the ith cycle is then the inverse $\eta_k^{-1}(i,m)$ of $\eta_k(i,m)$, ($k=1,2$, $i=1,\ldots,I$). In the sequel we shall represent the SM of Array k by the $M_k\times I$-dimensional matrix $\boldsymbol{\eta}_k=[\boldsymbol{\eta}_k(1),\ldots,\boldsymbol{\eta}_k(I)]$.

Employing the TDM mode in Fig. 2 and following the same notation as in [7], the scalar signal at the output of Sw2 reads

$$Y(t)=\sum_{\ell=1}^{L} s(t;\boldsymbol{\theta}_\ell)+\sqrt{\tfrac{N_0}{2}}q_2(t)W(t), \tag{3}$$

where $W(t)$ denotes standard complex white Gaussian noise and $q_2(t)$ is an indicator function, i.e. with range $\{0,1\}$, which takes value one if, and only if, some element of the Rx array is connected to the output of Sw2. Moreover,

$$s(t;\boldsymbol{\theta}_\ell)=\alpha_\ell\exp\{j2\pi\nu_\ell t\}\boldsymbol{c}_2(\boldsymbol{\Omega}_{2,\ell})^{\mathrm{T}}\boldsymbol{U}(t;\tau_\ell)\boldsymbol{c}_1(\boldsymbol{\Omega}_{1,\ell}).$$

The definition of the $M_2\times M_1$ sounding matrix is $\boldsymbol{U}(t;\tau_\ell)\doteq\boldsymbol{q}_2(t)\boldsymbol{q}_1(t)^{\mathrm{T}}u(t-\tau_\ell)$, where $u(t)$ is the signal at the input of Sw1. The vector-valued functions $\boldsymbol{q}_k(t)$ characterizes the timing of Swk ($k=1,2$). More specifically, the m_kth entry of $\boldsymbol{q}_k(t)$ is an indicator function which takes value one, if and only if, Swk switches the m_kth element of Array k [7].

IV. Objective Function used in the Estimation of the DF and the Directions.

A. TDM MIMO Channel Sounding.

According to [1] and [2] at each iteration of the ISI-SAGE algorithm, the parameter estimates of the ℓth path are updated sequentially in the maximization (M-) step of the algorithm in an optimization procedure using an objective function equal to the absolute value of

$$z(\bar{\boldsymbol{\theta}}_\ell;\hat{x}_\ell)\doteq\tilde{\boldsymbol{c}}_2(\boldsymbol{\Omega}_{2,\ell})^{\mathrm{H}}\boldsymbol{X}_\ell(\tau_\ell,\nu_\ell;\hat{x}_\ell)\tilde{\boldsymbol{c}}_1(\boldsymbol{\Omega}_{1,\ell})^{*}, \tag{4}$$

where $\bar{\boldsymbol{\theta}}_\ell\doteq[\boldsymbol{\Omega}_{1,\ell},\boldsymbol{\Omega}_{2,\ell},\tau_\ell,\nu_\ell]$, $[\cdot]^{\mathrm{H}}$ denotes the Hermitian operator, $[\cdot]*$ represents the complex conjugate, and $\tilde{\boldsymbol{c}}_k(\boldsymbol{\Omega}_{k,\ell})\doteq|\boldsymbol{c}_k(\boldsymbol{\Omega}_{k,\ell})|^{-1}\boldsymbol{c}_k(\boldsymbol{\Omega}_{k,\ell})$ is the normalized response of Array k ($k=1,2$). Here, $|\cdot|$ is the Euclidean norm. The entries of the $M_2\times M_1$ dimensional matrix $\boldsymbol{X}_\ell(\tau_\ell,\nu_\ell;\hat{x}_\ell)$ read

$$X_{\ell,m_2,m_1}(\tau_\ell,\nu_\ell;\hat{x}_\ell)=\sum_{i=1}^{I}\Big[\exp\{-j2\pi\nu_\ell t_{i,m_1,m_2}\}\cdot\textstyle\int_0^{T_s}u^*(t-\tau_\ell)\exp\{-j2\pi\nu_\ell t\}\hat{x}_\ell(t+t_{i,m_1,m_2})\,\mathrm{d}t\Big], \tag{5}$$

$m_k=1,\ldots,M_k, k=1,2$. In (5) $\hat{x}_\ell(t)$ is an estimate of the hidden data $X_\ell(t)=s(t;\boldsymbol{\theta}_\ell)+\sqrt{\frac{N_0}{2}}q_2(t)W_\ell(t)$ [8], which is calculated in the expectation (E-) step of the ISI-SAGE algorithm to be $\hat{x}_\ell(t)=y(t)-\sum_{\ell'=1,\ell'\neq\ell}^{L}s(t;\hat{\boldsymbol{\theta}}_{\ell'}^{'})$, with $\hat{\boldsymbol{\theta}}_{\ell'}^{'}$ denoting the current estimate of $\boldsymbol{\theta}_{\ell'}$.

In the subsequent analysis of the behavior of the objective function versus the DF, the DoD and DoA we make the following four simplifying assumptions. Firstly, the phase change due to the DF within T_s is neglected, i.e. the term $\exp\{-j2\pi\nu_\ell t\}$ in (5) is set equal to 1. As shown in [3] this effect can be easily included into the model and its impact on the performance of the DF estimator proves to be negligible. Secondly, the propagation delay is known. Based on this assumption, $z(\bar{\boldsymbol{\theta}}_\ell,\hat{x}_\ell)$ reduces to a function of $\boldsymbol{\Omega}_{1,\ell}$, $\boldsymbol{\Omega}_{2,\ell}$, and ν_ℓ as

$$z(\nu_\ell,\boldsymbol{\Omega}_{1,\ell},\boldsymbol{\Omega}_{2,\ell};\hat{x}_\ell)=\sum_{i=1}^{I}\sum_{m_2=1}^{M_2}\sum_{m_1=1}^{M_1}\tilde{c}_{1,m_1}(\boldsymbol{\Omega}_{1,\ell})^{*}\tilde{c}_{2,m_2}(\boldsymbol{\Omega}_{2,\ell})^{*}\cdot\exp\{-j2\pi\nu_\ell t_{i,m_1,m_2}\}\textstyle\int_0^{T_s}u(t-\tau_\ell')^{*}\hat{x}_\ell(t+t_{i,m_1,m_2})\,\mathrm{d}t, \tag{6}$$

where τ_ℓ' is the true delay value. Thirdly, in updating the parameter estimates of the ℓth wave, the ISI-SAGE algorithm has perfectly estimated the parameters of the other waves. Thus, the E-step returns the estimate $\hat{x}_\ell(t)=s(t;\boldsymbol{\theta}_\ell)+\sqrt{\frac{N_0}{2}}q_2(t)W_\ell(t)$. With this assumption, in the M-step the estimation of the ℓth propagation path is based on a signal perfectly cleaned from the combination of the other waves (one-wave scenario). Finally, we assume that all antenna elements are isotropic.

Under these assumptions, by dropping constants, (6) can be cast as

$$z(\nu_\ell,\boldsymbol{\Omega}_{1,\ell},\boldsymbol{\Omega}_{2,\ell};\hat{x}_\ell)=\sum_{i=1}^{I}R_i(\check{\nu}_\ell)S_i(\check{\boldsymbol{\Omega}}_{1,\ell},\check{\nu}_\ell)T_i(\check{\boldsymbol{\Omega}}_{2,\ell},\check{\nu}_\ell)+V(\nu_\ell,\boldsymbol{\Omega}_{1,\ell},\boldsymbol{\Omega}_{2,\ell}), \tag{7}$$

where

$$\begin{aligned} R_i(\check{\nu}_\ell) &= \exp\{j2\pi\check{\nu}_\ell \left(i-\tfrac{I+1}{2}\right) T_{cy}\}, \\ S_i(\check{\boldsymbol{\Omega}}_{1,\ell},\check{\nu}_\ell) &= \sum_{m_1=1}^{M_1} \exp\{j2\pi\lambda_0^{-1}[\check{\boldsymbol{\Omega}}_{1,\ell}\cdot\boldsymbol{r}_{1,m_1}] \\ &\quad +j2\pi\check{\nu}_\ell \left(\eta_1(i,m_1)-\tfrac{M_1+1}{2}\right) T_t\}, \\ T_i(\check{\boldsymbol{\Omega}}_{2,\ell},\check{\nu}_\ell) &= \sum_{m_2=1}^{M_2} \exp\{j2\pi\lambda_0^{-1}[\check{\boldsymbol{\Omega}}_{2,\ell}\cdot\boldsymbol{r}_{2,m_2}] \\ &\quad +j2\pi\check{\nu}_\ell \left(\eta_2(i,m_2)-\tfrac{M_2+1}{2}\right) T_r\}, \end{aligned}$$

and, $\check{\nu}_\ell = \nu'_\ell - \nu_\ell$, $\check{\boldsymbol{\Omega}}_{1,\ell} = \boldsymbol{\Omega}'_{1,\ell} - \boldsymbol{\Omega}_{1,\ell}$, and $\check{\boldsymbol{\Omega}}_{2,\ell} = \boldsymbol{\Omega}'_{2,\ell} - \boldsymbol{\Omega}_{2,\ell}$ with ν'_ℓ, $\boldsymbol{\Omega}'_{1,\ell}$ and $\boldsymbol{\Omega}'_{2,\ell}$ denoting the true parameters. The noise term $V(\nu_\ell,\boldsymbol{\Omega}_{1,\ell},\boldsymbol{\Omega}_{2,\ell})$ can be derived analogously to $V(\nu_\ell)$ in [3]. Notice that the expressions given as arguments of the exponential terms in the summands of $S_i(\check{\boldsymbol{\Omega}}_{1,\ell},\check{\nu}_\ell)$ and $T_i(\check{\boldsymbol{\Omega}}_{2,\ell},\check{\nu}_\ell)$ reflect a coupling between the DoD and the DF and between the DoA and the DF respectively.

B. Case Study: TDM Single-Input Multiple-Output (SIMO) Channel Sounding with Uniform Linear Array.

In this case the DoDs cannot be estimated and (7) reduces to

$$z(\nu_\ell,\boldsymbol{\Omega}_{2,\ell};\hat{x}_\ell)=\sum_{i=1}^{I} R_i(\check{\nu}_\ell)T_i(\check{\boldsymbol{\Omega}}_{2,\ell},\check{\nu}_\ell)+V(\nu_\ell,\boldsymbol{\Omega}_{2,\ell}). \quad (8)$$

The absolute value of the right-hand expression in (8) is the objective function for the calculation of the estimates $\hat{\nu}_\ell$ and $\hat{\boldsymbol{\Omega}}_{2,\ell}$. As a special case, we investigate the behavior of (8) in the noiseless case ($V(\nu_\ell,\boldsymbol{\Omega}_{2,\ell}) = 0$) when the uniform linear Rx array consists of M_2 isotropic antennas with locations $\boldsymbol{r}_{2,m_2} = [\frac{m_2\lambda_0}{2},0,0]^{\mathrm{T}}$, $m_2 = 1,\ldots,M_2$. The inner products arising in the response of this array are calculated to be $\boldsymbol{\Omega}_{2,\ell}\cdot\boldsymbol{r}_{2,m_2} = \cos(\psi_\ell)\frac{m_2\lambda_0}{2}$, $m_2 = 1,\ldots,M_2$, where ψ_ℓ designates the angle between the impinging direction of the ℓth wave and the array axis. It is a well-known fact that ψ_ℓ is the only characteristic of $\boldsymbol{\Omega}_{2,\ell}$ that can be estimated unambiguously with these types of arrays. Notice that $\cos(\psi_\ell) \doteq \cos(\phi_{2,\ell})\sin(\theta_{2,\ell})$. For simplicity, we consider a cycle-independent SM $\boldsymbol{\eta}_2(i) = \boldsymbol{\eta}_2, i = 1,\ldots,I$. In this case, the absolute value of (8) reads

$$\begin{aligned} |z(\nu_\ell,\boldsymbol{\Omega}_{2,\ell};\hat{x}_\ell)| &= |z(\check{\nu}_\ell,\check{\psi}_\ell;\hat{x}_\ell)| \\ &= \left|T(\check{\psi}_\ell,\check{\nu}_\ell)\right|\cdot|G(\check{\nu}_\ell)|, \end{aligned} \quad (9)$$

where $\check{\psi}_\ell = \cos(\psi'_\ell) - \cos(\psi_\ell)$ with ψ'_ℓ denoting the true value and

$$\begin{aligned} T(\check{\psi}_\ell,\check{\nu}_\ell) &\doteq \frac{1}{M_2}\sum_{m_2=1}^{M_2} \exp\{jm_2\pi\check{\psi}_\ell \\ &\quad +j2\pi\check{\nu}_\ell[\eta_2(m_2)-\tfrac{M_2+1}{2}]T_r\}, \\ G(\check{\nu}_\ell) &\doteq \frac{\sin(\pi\check{\nu}_\ell I T_{cy})}{I\sin(\pi\check{\nu}_\ell T_{cy})} \quad . \end{aligned}$$

Notice that the cycle-independent SMs affect only the term $T(\check{\psi}_\ell,\check{\nu}_\ell)$ in the objective function.

As an illustration, Fig. 3 depicts the graphs of $|G(\check{\nu}_\ell)|$ (top), $|T(\check{\psi}_\ell,\check{\nu}_\ell)|$ (middle), and $|z(\check{\nu}_\ell,\check{\psi}_\ell;\hat{x}_\ell)|$ (bottom) in (9) for the parameter setting specified in Table I when a (cycle-independent) sequential SM, $\boldsymbol{\eta}_2(i) = [1,2,\ldots,8]^{\mathrm{T}}, i = 1,\ldots,I$ is applied. The range of $\check{\nu}_\ell$ is $\pm\frac{1}{2T_r} = \pm 200$ Hz. Clearly, the function $|G(\check{\nu}_\ell)|$ is periodic with period $\frac{1}{T_{cy}}$. The

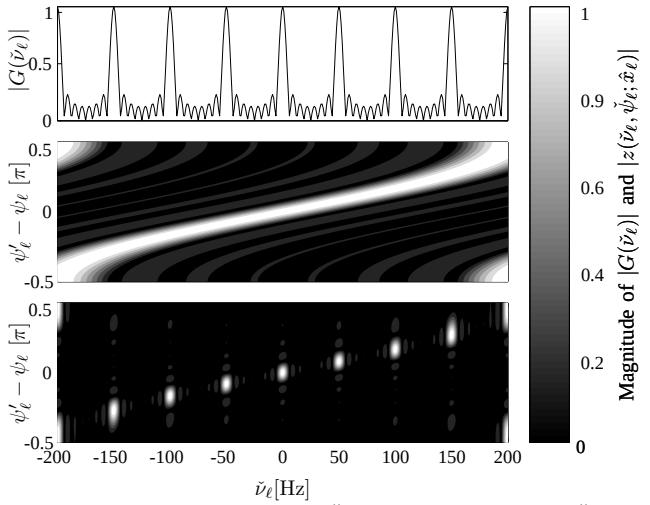

Fig. 3. The graphs of $|G(\check{\nu}_\ell)|$ (top), $|T(\check{\psi}_\ell,\check{\nu}_\ell)|$ (middle) and $|z(\check{\nu}_\ell,\check{\psi}_\ell;\hat{x}_\ell)|$ (bottom) for the parameter setting reported in Table I when the sequential SM $\boldsymbol{\eta}_2(i) = [1,2,\ldots,8]^{\mathrm{T}}, i = 1,\ldots,I$ is applied. Notice that the range of $(\psi'-\psi)$ is $\left[-\frac{\pi}{2},\frac{\pi}{2}\right]$.

locus of the pairs $(\check{\nu}_\ell,\check{\psi}_\ell)$ where $T(\check{\psi}_\ell,\check{\nu}_\ell)$ reaches its maximum value $(=1)$ is the curve $\psi'_\ell - \psi_\ell = \frac{\pi}{2} - \mathrm{Arc}\cos(2\check{\nu}_\ell T_r)$. As apparent in the bottom plot, the product of the above two functions, i.e. $|z(\check{\nu}_\ell,\check{\psi}_\ell;\hat{x}_\ell)|$, exhibits multiple maxima separated by $\frac{1}{T_{cy}} = 50$ Hz in $\check{\nu}$ along the above curve. Notice that $|z(\check{\nu}_\ell,\check{\psi}_\ell;\hat{x}_\ell)|$ exhibits one unique maximum if $\check{\nu}_\ell$ is restricted to the range $\pm\frac{1}{2T_{cy}}$. In this case there is no ambiguity in the estimation of the DF and the DoA. If the DF estimation range is extended to $\pm\frac{1}{2T_r}$ and the switch of the sounding system uses the sequential SM, an ambiguity in the estimation of the parameters occurs due to the multiple maxima of the objective function.

C. Method to Avoid the Ambiguity Problem

In this subsection we show that the ambiguity problem of the case study can be avoided by suitably selecting the

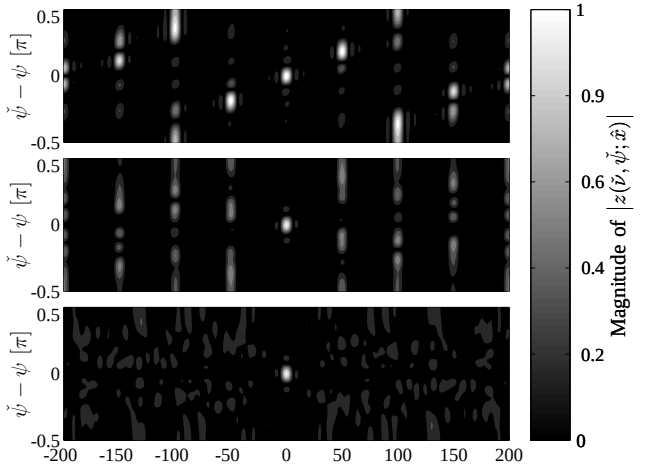

Fig. 4. Contour plot of normalized objective functions, for the parameter setting listed in Table I. The top, middle and bottom plots correspond respectively to the modulo-type SM $\boldsymbol{\eta}_2(i) = [1,3,5,7,2,4,6,8]^{\mathrm{T}}, i = 1,\ldots,I$, the non-modulo-type SM $\boldsymbol{\eta}_2(i) = [4,2,1,8,5,7,3,6]^{\mathrm{T}}, i = 1,\ldots,I$, both repeated over the 8 cycles, and 8 different non-modulo-type SMs selected randomly among all permutations.

I	M_1	M_2	T_{cy}[s]	ν'[Hz]	ψ'[rad]
8	1	8	0.02	0	$\frac{\pi}{2}$

TABLE I
SIMULATION SETTING FOR SIMO SYSTEMS

SMs. The considered situation is specified in Table I. The index ℓ is omitted from here on. We define a modulo-type SM to be an SM that its entries $\eta_2(m_2)$ fulfill the identities $(\eta_2(m_2)-1) = Jm_2 + K \pmod{M_2}$, $m_2 = 1,\ldots,M_2$ and $K = 0,1,\ldots,M_2-1$ for some integer J such that J and M_2 are mutually non-divisible, i.e. $J \nmid M_2 \wedge M_2 \nmid J$, where $\nmid$ means "is not a divisor of". Notice that the sequential SM $\boldsymbol{\eta}_2(i) = [1,2,\ldots,8]^{\mathrm{T}}, i = 1,\ldots,I$ is a modulo-type SM with $J = 1$ and $K = 0$. It can be shown that all modulo-type SMs lead to an objective function exhibiting multiple maxima. Fig. 4 depicts the objective function $|z(\check{\nu},\check{\psi};\hat{x})|$ in (9) normalized by IM_2, using the cycle-independent modulo-type SM $\boldsymbol{\eta}_2(i) = [1,3,5,7,2,4,6,8]^{\mathrm{T}}, i = 1,\ldots,I$ (top), the cycle-independent SM $\boldsymbol{\eta}_2(i) = [4,2,1,8,5,7,3,6]^{\mathrm{T}}, i = 1,\ldots,I$ (middle), and a cycle-dependent SM with different randomly selected non-modulo-type SMs for each cycle (bottom). For the modulo-type SM, the objective function exhibits multiple maxima, while it exhibits a single maximum located at $(\check{\nu},\check{\psi}) = (0,0)$ in the two other cases. Furthermore, the bottom plot shows that the amplitudes of the side-lobes of $|z(\check{\nu},\check{\psi};\hat{x})|$ can be further reduced by using cycle-dependent SMs.

V. EXPERIMENTAL INVESTIGATIONS

In this section, we present experimental investigations that illustrate the effect of the switching mode on the objective function used in the ISI-SAGE algorithm to estimate the DF. The measurements have been performed with the TDM-MIMO channel sounder PROPSound [9]. The Tx array consists of 3 conformal sub-arrays of 8 dual-polarized patches uniformly spaced on a cylinder together with a uniform rectangular 2×2 sub-array of 4 similar dual-polarized patches placed on top of the cylinder ($M_1 = 54$). At the Rx a 4×4 planar array with 16 dual-polarized patches is used ($M_2 = 32$). The spacing between the Rx array elements and the elements of the four Tx sub-arrays is half a wavelength. The selected carrier frequency is 2.45 GHz. The sounding signal of power 100 mW is a pseudo-noise (PN) sequence of length $K = 255$ chips with chip duration $T_c = 10$ ns. The sensing interval coincides with one period of the PN-sequence, i.e. $T_s = KT_c = 2.55$ μs.

The Rx array was mounted outside a window on the 3rd floor of the Elektrobit AG building in Bubikon, Switzerland. The Tx array was mounted on the roof of a van moving with approximately 8 m/s away from the building. The measurements were performed twice along the same route with different measurement settings. The van was driving at approximately the same velocity in both cases to ensure almost identical DFs in the two measurement scenarios. The DF of the LOS path can be calculated from the geometrical configuration and the van velocity to be approximately -59 Hz. The selected parameter settings specific to the two measurements are reported in Table. II. They have been selected in such a way that the DF of the LOS path is in the range of $[-\frac{1}{2T_{cy}},\frac{1}{2T_{cy}}]$ in Case I but not in Case II. However in the latter case, the DF lies in the range $[-\frac{1}{2T_r},\frac{1}{2T_r}]$. As we will see in the sequel, the SM at the Tx is irrelevant in the situation. At the Rx, we apply a patch-wise sequential SM in Case I and a patch-wise non-modulo-type SM in Case II. The term "patch-wise" indicates that due to some technical constraints, the two elements of each patch are always switched consecutively.

The ISI-SAGE algorithm was applied to estimate the individual parameter vectors of $L = 4$ propagation paths using $I = 4$ measurement cycles. The parameter estimates of the four paths are initialized successively with an Non-Coherent Maximum Likelihood (NC-ML) [10] technique. It can be shown that the objective function used for the joint initialization of ν_ℓ and $\boldsymbol{\Omega}_{2,\ell}$ after the delay initialization $\tau_\ell = \hat{\tau}_\ell(0)$ has been computed is similar to the squared absolute value of (8) with $\tau_\ell = \hat{\tau}_\ell(0)$ and $\hat{x}_\ell(t) = y(t) - \sum_{\ell'=1}^{\ell-1} s(t;\hat{\boldsymbol{\theta}}'_{\ell'}(0))$. Notice that since at that stage, the DoD of the ℓth path has not been estimated, the SM at the Tx is irrelevant in the NC-ML technique used to initialize $\hat{\nu}_\ell$ and $\hat{\boldsymbol{\Omega}}_\ell$. Hence, we can use the initialization procedure of the ISI-SAGE algorithm to investigate experimentally a scenario similar to the case study described in subsection IV-B. The differences between the case study and the experimental investigation are as follows: (1) the SIMO scheme adopted in the case study is replaced by the MIMO scheme in the experimental investigation; (2) a planar array with dual-polarized elements is used instead of a linear uniform array and (3), the array elements are not isotropic. The response of the arrays, which have been assessed experimentally by means of calibration measurements, embody the directivity of the elements as well as the coupling between them. Notice that in the normal iterations, the E- and M-steps are performed as described in [1] and [2].

In the sequel we restrict the attention to the LOS path, which is ranked Number 1. To visualize the behavior of the objective function versus ν_1, we compute $F(\nu_1) \doteq \max_{\boldsymbol{\Omega}_{2,1}} |z(\nu_1,\boldsymbol{\Omega}_{2,1};\hat{x}_1 = y)|^2$ where the z function has a similar expression as (8) with $T_i(\check{\boldsymbol{\Omega}}_{2,1},\check{\nu}_1)$ depending on the response of the array at the Rx. Notice that we assume a one-wave scenario since in this particular experiment, the wave following the LOS path is the dominant part of the received signal. To understand the behavior of $F(\nu_1)$ theoretically, we insert (8) with the noise term omitted in the definition of this function and obtain in this way:

$$F(\nu_1) \quad = \quad \max_{\check{\boldsymbol{\Omega}}_{2,1}} |\sum_{i=1}^{I} R_i(\check{\nu}_1) T_i(\check{\boldsymbol{\Omega}}_{2,1},\check{\nu}_1)|^2$$

	Case I	Case II
$T_r[\mu$s]	3.05	5.10
$[-\frac{1}{2T_r},\frac{1}{2T_r}]$ [kHz]	$[-163.934, 163.934]$	$[-98.039, 98.039]$
T_{cy} [ms]	6.2	47.2
$[-\frac{1}{2T_{cy}},\frac{1}{2T_{cy}}]$ [Hz]	$[-81.3, 81.3]$	$[-10.6, 10.6]$
SM at the Rx	Patch-wise Sequential SM	Patch-wise Non-modulo-type SM

TABLE II
MEASUREMENT SETTINGS FOR CASE I AND CASE II

$$
\begin{aligned}
&= \max_{\check{\boldsymbol{\Omega}}_{2,1}} |G(\check{\nu}_1) T(\check{\boldsymbol{\Omega}}_{2,1}, \check{\nu}_1)|^2 \\
&= \max_{\check{\boldsymbol{\Omega}}_{2,1}} |T(\check{\boldsymbol{\Omega}}_{2,1}, \check{\nu}_1)|^2 \cdot |G(\check{\nu}_1)|^2 \\
&= |T'(\check{\nu}_1)|^2 \cdot |G(\check{\nu}_1)|^2. \qquad (10)
\end{aligned}
$$

The second line is similar to (9) since the SM is cycle-independent. Furthermore $T'(\check{\nu}_1) \doteq \max_{\check{\boldsymbol{\Omega}}_{2,1}} T(\check{\boldsymbol{\Omega}}_1, \check{\nu}_1)$. Notice that a cycle-independent SM affects $F(\nu_1)$ via $|T'(\check{\nu}_1)|^2$.

The function $F(\nu_1)$ is depicted in Fig. 5 (top) for ν_1 ranging in $[-81.3\,\text{Hz}, 81.3\,\text{Hz}]$ for Case I and Case II. The pulse-train-like behavior observed in the two curves is due to the effect of $|G(\check{\nu}_1)|^2$, which is periodic with period $1/T_{cy}$. The maximum of $F(\nu_1)$ in Case I with the DF estimation range equal to $[-\frac{1}{2T_{cy}}, \frac{1}{2T_{cy}}]$, is located at -52 Hz. In Case II, with the DF estimation range extended to $[-\frac{1}{2T_r}, \frac{1}{2T_r}]$, the maximum of $F(\nu_1)$ is located at -81 Hz. Notice that these values are the initial estimates of the DF of the LOS path returned by the ISI-SAGE algorithm. After four iterations of the ISI-SAGE algorithm, the estimate $\hat{\nu}_1$ of the DF of the LOS path has converged to -52.5 Hz in Case I when the DF estimation range is confined to $[-\frac{1}{2T_{cy}}, \frac{1}{2T_{cy}}]$, and to -60 Hz in Case II where the DF estimation range equals $[-\frac{1}{2T_r}, \frac{1}{2T_r}]$. Both values are in accordance with the theoretically calculated value of -59 Hz. The difference of the two estimates is due to the difference in velocities with which the van was driving. In case the range of DF estimation is extended to $[-\frac{1}{2T_r}, \frac{1}{2T_r}]$ in Case I, the maximum of $F(\nu_1)$ is located at -97.604 kHz in the initialization step (as shown in Fig. 5 (bottom)), and stays at this value after 4 iterations. This estimate is obviously an artifact that results from the ambiguity effect due to the patch-wise sequential switching of the Rx array.

The pulse-train-like behavior of the function $F(\nu_1)$ due to $|G(\nu_1)|^2$ results in $\frac{T_{cy}}{T_r}$ peaks in the range $[-\frac{1}{2T_r}, \frac{1}{2T_r}]$ (i.e. approximately 2 000 and 10 000 peaks for Case I and Case II respectively). This feature makes it difficult to distinguish details of $F(\nu_1)$ when plotted in the above range. Therefore, for simplicity we calculate $\mathrm{Env}(F(\nu_1))$, as an approximation of $|T'(\check{\nu}_1)|^2$. Here $\mathrm{Env}(\cdot)$ refers to a pseudo-envelope (PE) curve which is obtained by dividing the range of ν_1 into multiple bins with an equal width of $\frac{1}{T_{cy}}$ and connecting the maxima of $F(\nu_1)$ from each bin by linear interpolation. Since $T_i(\check{\boldsymbol{\Omega}}_{2,1}, \check{\nu}_1)$ is the only term in the objective function that is affected by $\boldsymbol{\eta}_2$ when using cycle-independent SMs, the reported PE curve illustrates the effect of the different SMs on the objective function. Fig. 5 (bottom) reports the PE curves for Case I and Case II respectively. Notice that the DF axis has been normalized with respect to T_r for the two different cases. It can be observed that the curve obtained for Case I remains close to one over the DF range $\left[-\frac{1}{2T_r}, \frac{1}{2T_r}\right]$. This behavior is due to the ambiguity problem stemming from the sequential SM used for the 4×4 planar array. For Case II, the curve exhibits a dominant lobe with maximum height and multiple side-lobe with much lower amplitude. Thus, the ambiguity is effectively avoided. Furthermore, the distance of the zero points of the main lobes can be calculated theoretically to be $\frac{2}{M_2} = 0.066$ with respect to the normalized DF $(\nu_1 \cdot T_r)$, in accordance with the observation shown in the plot. Notice that the high side-lobes at the boundary of the DF estimation range are due to the patch-wise switching of the arrays. In the case the DF is very low compared to the switching rate, the resulting phase-shift due to the DF between consecutive sensing intervals of the elements of a patch is almost zero, which leads to an effective doubling of T_r. Since the DF is much smaller than $\frac{1}{2T_r}$ in the investigated case, the graph of $\mathrm{Env}(F(\nu_1))$ exhibits two segments that have a similar shape as shown in Fig. 5 (bottom).

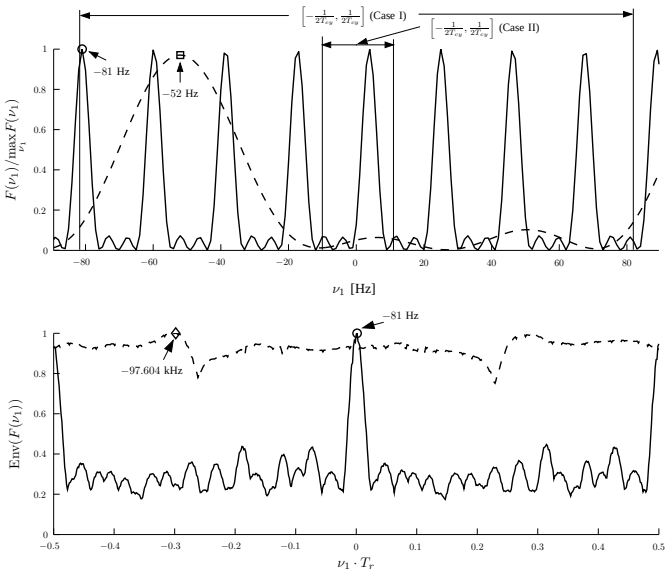

Fig. 5. Graph of the normalized $F(\nu_1)$ (top) and its pseudo-envelope $\mathrm{Env}(F(\nu_1))$ (bottom) obtained with the measured data in Case I (dashed lines) and Case II (solid lines). The mark $\circ$ denotes the maximum of $F(\nu_1)$ for Case II. The marks $\square$ and $\diamond$ denote the maxima of $F(\nu_1)$ when the DF estimation range is respectively $\left[-\frac{1}{2T_{cy}}, \frac{1}{2T_{cy}}\right]$ and $\left[-\frac{1}{2T_r}, \frac{1}{2T_r}\right]$ for Case I.

The above investigation shows experimentally the ambiguity effect that occurs when the DF estimation range is extended to $[-\frac{1}{2T_r}, \frac{1}{2T_r}]$ and the sequential SM is used. It also demonstrates that this problem is avoided when a specific (non-modulo-type) patch-wise SM is used.

VI. Conclusion

In this contribution, the behavior of the DF and direction estimates obtained with the ISI-SAGE algorithm described in [1] and [2] is investigated when the TDM scheme is applied in combination with channel sounding using switched multiple Tx and Rx antennas. A theoretical analysis combined with simulations show that when the DF estimation range is selected larger than half the measurement cycle rate as proposed in [3], so-called modulo-type switching modes (SMs) used with uniform linear and planar arrays lead to an ambiguity in the estimation of the DF and the directions DoA and DoD. Theoretical and experimental investigations show that the ambiguity problem can be avoided by applying specific SMs.

References

[1] B. H. Fleury, X. Yin, K. G. Rohbrandt, P. Jourdan, and A. Stucki, "High-resolution bidirection estimation based on the SAGE algorithm: Experience gathered from field experiments," *Proc. XXVIIth General Assembly of the Int. Union of Radio Scientists (URSI).* # 2127, 2002.

[2] ——, “Performance of a high-resolution scheme for joint estimation of delay and bidirection dispersion in the radio channel,” *Proc. IEEE Vehicular Technology Conference, VTC 2002 Spring*, pp. 522–526, 2002.
[3] X. Yin, B. H. Fleury, P. Jourdan, and A. Stucki, “Doppler frequency estimation for channel sounding using switched multiple transmit and receive antennae,” *Proc. IEEE Global Communications Conference, Globecom2003*, 2003.
[4] I. E. Telatar, “Capacity of multi-antenna gaussian channels,” *European Transactions on Telecommunication*, vol. 10, pp. 585–595, 1999.
[5] G. J. Foschini and M. J. Gans, “On limits of wireless communications in a fading environment when using multiple antennas,” *Wireless Personal Communications*, vol. 6, pp. 311–335, 1998.
[6] D. Chizhik, G. J. Foschini, and R. A. Valenzuela, “Capacities of multi-element transmit and receive antennas: Correlations and keyholes,” *IEE Electronics Letters*, vol. 36, no. 13, pp. 1099–1100, June 2000.
[7] B. H. Fleury, P. Jourdan, and A. Stucki, “High-resolution channel parameter estimation for MIMO applications using the SAGE algorithm,” *2002 Int. Zurich Seminar on Broadband Communications*, vol. 30, pp. 1–9, 2002.
[8] B. H. Fleury, M. Tschudin, R. Heddergott, D. Dahlhaus, and K. L. Pedersen, “Channel parameter estimation in mobile radio environments using the SAGE algorithm,” *IEEE Journal on Selected Areas in Communications*, vol. 17, no. 3, pp. 434–450, Mar. 1999.
[9] A. Stucki *et. al.*, “PropSound System Specifications Document: Concept and Specifications,” Elektrobit AG, Switzerland,” Internal Report, 2001.
[10] X. Yin, B. H. Fleury, P. Jourdan, and A. Stucki, “Polarization estimation of individual propagation paths using the sage algorithm,” *The 14th IEEE International Symposium on Personal, Indoor and Mobile Radio Communications, PIMRC2003)*, 2003.